Testing Realism of Software Breast Phantoms: Texture Analysis of Synthetic Mammograms

Predrag R. Bakic, Brad Keller, Yuanjie Zheng, Yan Wang, James C. Gee, Despina Kontos, and Andrew D. A. Maidment

Department of Radiology, University of Pennsylvania, Philadelphia, PA 19104

{ Predrag.Bakic, Brad.Keller , Yuanjie.Zheng , GeeJames , Despina.Kontos , Andrew.Maidment }@uphs.upenn.edu; WangYan1@sas.upenn.edu

ABSTRACT

Software breast phantoms have been developed for pre-clinical validation of breast imaging systems. Realism is of great importance for the acceptance and the range of applications of breast phantoms. In this paper we have assessed the phantom realism based upon the analysis of mammographic texture properties. Texture analysis is of interest since it reflects the spatial tissue distribution, which is known to correlate with breast cancer risk. We compared texture properties of synthetic mammograms generated using software breast phantoms with clinical data. A total of 133 phantom images were synthesized using software phantoms developed at the University of Pennsylvania. The phantoms were designed using two different anatomy simulation methods: an octree-based recursive partitioning method and a region growing method. The synthetic images were generated assuming a clinically used acquisition geometry and mono-energetic x-ray beam with no scatter. The clinical data included 60 anonymized mammograms selected retrospectively from screening cases at the University of Pennsylvania. The same postprocessing was applied to clinical and phantom images. The texture analysis was performed using fully automated software which extracts a battery of features from analyzed images. The histograms of texture properties extracted from phantom images were compared with those from clinical mammograms, separately for the two anatomy simulation methods. The histogram agreement was quantified using symmetrized Kulback-Leibler divergence. We observed good agreement for most of the analyzed 25 features. In more than a half of the features, the octree-based simulation method yielded better agreement with clinical data as compared with the region growing method.

Keywords: Breast anatomy simulation, software breast phantoms, parenchymal texture analysis, realism assessment, histogram comparison.

1. INTRODUCTION

Recent years have seen a significant increase in the use of software breast phantoms for pre-clinical validation of breast imaging systems. Our breast anatomy simulation software has been developing since 1996,[1-6] and today is in use by over 40 industrial, government, and academic research laboratories. Other approaches to the software breast phantom design have been reported.[7-11] Fig. 1 shows cross-sections of examples from different generations of software phantoms developed at the University of Pennsylvania. The current phantom design is based upon the use of octrees, which provides very fast simulation.[12]

There are several important motivations for the use of software breast phantoms. Software phantoms provide direct simulation of tissue structures which make up anatomical noise, *i.e.*, the background texture seen in clinical images, which affects the ability of observers to detect and characterize breast abnormalities. Phantoms allow consistent simulation of images of the same anatomy while varying the acquisition parameters. Phantoms also provide ground truth about the simulated anatomical structures, which is needed for quantitative validation. They are also flexible enough to cover the wide anatomical variations seen in clinical images. Lastly, they are suitable for use in virtual clinical trials (VCT) of breast imaging systems. The validation of breast imaging systems is currently based upon clinical trials, which are limited by their cost, duration, and necessity for repeated irradiation of volunteer women (in case of imaging modalities based upon the ionizing radiation). The X-ray Physics Laboratory at the University of

Medical Imaging 2013: Physics of Medical Imaging, edited by Robert M. Nishikawa, Bruce R. Whiting, Christoph Hoeschen,
Proc. of SPIE Vol. 8668, 866824 · © 2013 SPIE · CCC code: 1605-7422/13/$18 · doi: 10.1117/12.2008173

Pennsylvania is a strong proponent of a preclinical alternative in the form of VCTs based upon the models of anatomy, image acquisition (and optionally) image analysis.

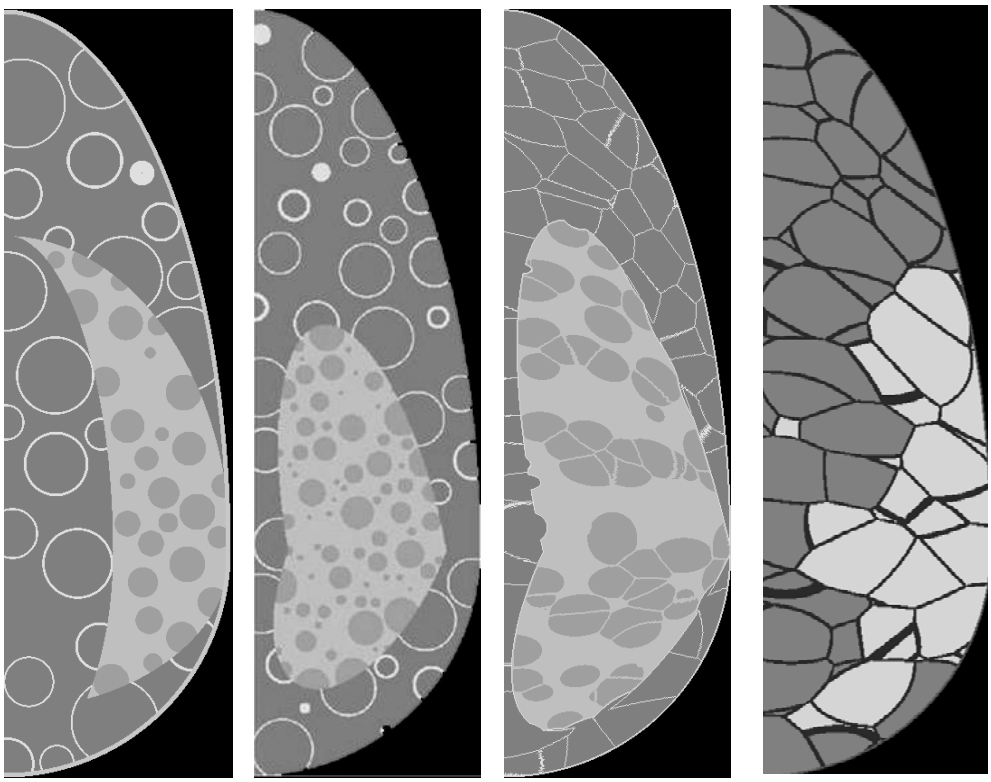

(a) (b) (c) (d)

Figure 1: Illustration of the changes in design of software breast phantoms developed at the University of Pennsylvania. Shown are the cross-sections of phantoms from (a) 2002; (b) 2006; (c) 2010; and (d) 2012.

Realism is of great importance for the acceptance and the range of applications of software breast phantoms. Phantom realism may be assessed directly or indirectly. Direct assessment is performed by comparing phantoms and tissue properties using anatomical or pathological slices; this approach is limited by the available clinical material. In contrast, indirect realism assessment includes comparison of clinical and simulated phantom images.

This work is motivated by a desire to develop an automated tool for testing realism as a part of an open source platform for breast imaging simulation. The automated validation is envisioned to include: (i) Regression tests aimed to catch programming bugs early and (ii) Comparison of phantom vs. clinical images to ensure the highest available level of realism. The image-based features which can be used for the assessment of realism in phantom images include the estimates of breast percent density and parenchymal texture descriptors, covariance properties, and power spectral descriptors.

Texture analysis has been used for testing realism in earlier versions of our software breast phantom. In our 2002 study,[2] we analyzed the similarity between distributions of texture feature values averaged over image regions in synthetic and clinical breast images. Two similarity measures were utilized: (i) The histogram correlation of phantom and clinical texture features averaged over the same tissue regions; this measure was used to validate the distribution of texture feature values within individual simulated images; and (ii) the Kolmogorov-Smirnov test between cumulative density functions of mean texture features from phantom and clinical data; this measure was used to validate the distribution of mean texture features over the simulated population. Fig. 2 illustrates the use of these measures for the assessment of realism in simulated images of our previous software phantoms.

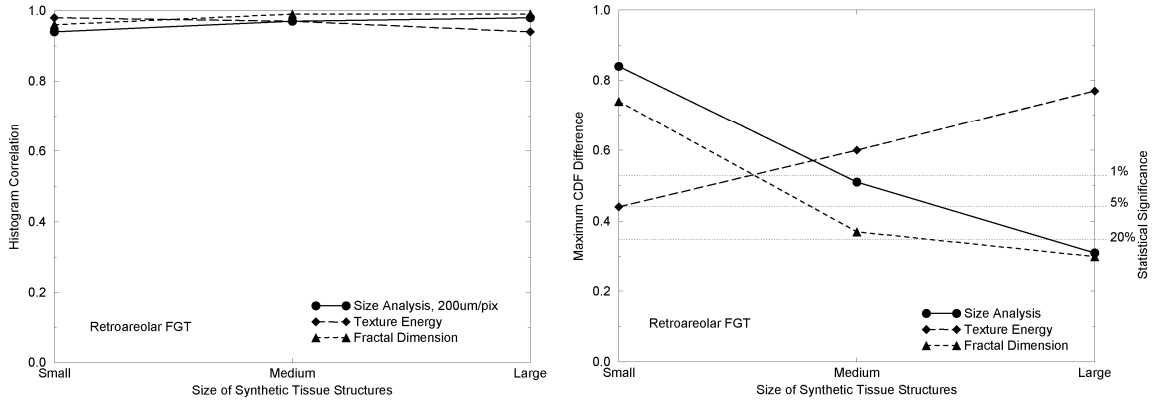

Figure 2: Examples of the texture analysis of synthetic images generated using an earlier version of our software breast phantom. Shown are (a) the correlation of texture histograms and (b) the Kolmogorov-Smirnov test of the difference between cumulative distributions of the mean texture values, for regions of retroareolar fibroglandular tissue. The data are presented for three ranges of size of synthetic tissue structures and for the three texture analysis methods. *(Modified from Ref. #2.)*

In this paper, we assessed the agreement between synthetic and clinical images by comparing histograms of various texture features. The histogram comparison was quantified using symmetrized Kulback-Leibler divergence.[13, 14] In addition, we separately compared the agreement with clinical data for images of software phantoms generated using the octree and region growing simulation methods.

2. METHODS

2.1. Software breast phantoms

The X-ray Physics Lab at the University of Pennsylvania has over 15 years of experience in developing breast anthropomorphic software phantoms.[1-6, 12, 15, 16] Phantoms are generated algorithmically using geometric primitives, and stored in a 3D voxel array at a spatial resolution selected by the user. Each voxel belongs to a unique simulated tissue structure, characterized by corresponding physical properties (e.g., linear x-ray attenuation, elasticity, etc.). Particular attention is given to the simulation of large- and meso-scale tissue structures, as breast outline, skin, and adipose tissue compartments, defined by the matrix of Cooper's ligaments. These structures make up the parenchymal pattern, a background image texture which can interfere with the detection of breast abnormalities. The anthropomorphic software phantoms used in this study are based upon two different methods for the simulation of breast anatomy: (i) recursive partitioning of the simulated breast volume using octrees[12] and region growing simulation method. [15, 16]

2.1.1 Octree-based method for the simulation of breast anatomy

The octree-based simulation[12] allows for fast generation of phantoms with very small voxel size. It is an upgrade to the previous region growing method, offering important advantages of (i) low computational complexity, (ii) fast, (iii) scalable, and (iv) an improved control of simulated anatomical structures (e.g., skin and Cooper's ligament thickness). The improved control of the simulation is provided through selection of input parameters which specify the simulated breast size, glandularity, thickness of the skin and Cooper's ligaments, and the number, distribution, and size and shape of adipose compartments.

2.1.2 Region growing method for the simulation of breast anatomy

In the region growing method,[15, 16] we divided the breast into a region composed predominantly of adipose tissue and a region composed predominantly of fibro-glandular tissue. Each compartment in the predominantly adipose tissue region is assigned an ellipsoid, centered at a randomly chosen seed point, with semiaxes which grow proportional to a virtual time $\tau \geq 0$. Ellipsoid parameters determine the orientation and relative size and shape of the compartments. Each voxel is assigned as belonging to a compartment corresponding to a seed of the ellipsoid that first reaches the voxel during the growing procedure. It can be shown that compartment boundaries generated by the region growing method represent

Voronoi diagrams with respect to the Mahalanobis distance. Fig. 3 shows cross-sections of sample software breast phantoms used in this study.

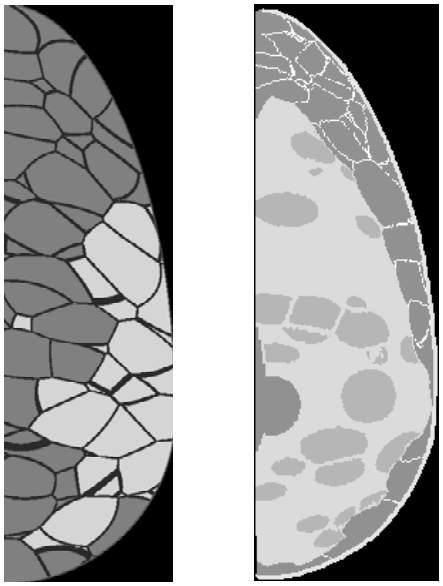

(a) (b)

Figure 3: Examples of phantoms used in this study. Shown are cross-sections of phantoms generated by (a) octree or (b) region growing simulation method.

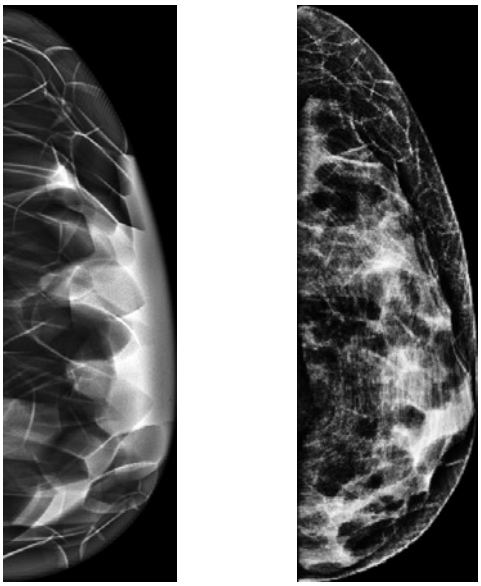

(a) (b)

Figure 4: Examples of synthetic mammograms used in this study, generated from the (a) octree-based phantoms or (b) regions growing phantoms.

2.2. Simulation of mammographic image acquisition

Synthetic images for this study were generated in a two-step model of mammographic image acquisition. First, software phantoms are deformed using a finite-element (FE) model of clinical mammographic compression. The FE model assumed hyper-elastic, almost uncompressible tissue model, with 50% reduction in phantom thickness. Second, the acquisition geometry corresponding to a clinical digital mammography system (Dimensions, HOLOGIC, Bedford, MA) was simulated by ray tracing. We assumed mono-energetic x-ray beam without scatter, and an ideal detector model. The quantum noise was added in the form of Poisson random variations to the digital pixel values. The simulated images were post-processed using the proprietary method provided by Hologic (courtesy of B. Ren and A. Smith). Fig. 4 shows examples of synthetic mammograms generated using octree and region growing phantoms.

2.3. Materials

2.3.1 Clinical mammograms

Clinical images used in this paper were selected retrospectively from breast cancer screening cases at the University of Pennsylvania, under HIPAA and IRB approval. We selected 60 clinical mammograms acquired using the HOLOGIC Dimensions system; the same system was modeled when generating synthetic images. None of the selected clinical images included confirmed breast abnormalities. Fig. 5 shows an example of clinical mammograms used in this study.

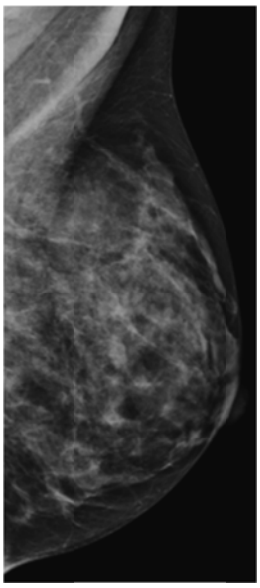

Figure 5: Example of a clinical mammograms used in this study.

2.3.2 Phantom images

Total of 133 phantom images were synthesized for the use in this study. Each image was synthesized from a unique phantom. Sixty-six phantoms were generated by the octree-based method and 67 by the region growing method. Both methods simulated phantoms of two volumes: 450 or 700 ml. The phantom volumetric density ranged between 20 and 40 percent. The octree phantoms were generated using the voxel size of 200 μm, while the region growing phantoms used the voxel size of 500 μm.

2.4. Texture analysis of synthetic and clinical images

The texture analysis was performed using a fully automated software pipeline,[17, 18] (Fig. 6) which extracts a battery of features from analyzed full-field digital mammography or digital breast tomosynthesis images. The pipeline includes an initial image quality test of the DICOM header files to validate that acceptable dose and image acquisition parameters were used (i.e., kVp, exposure, compression, etc.). A subsequent preprocessing step provides an option to create a regional tissue mask (i.e., by segmenting specific regions, as the dense and the fatty tissue regions) from which the parenchymal pattern descriptors are extracted. The pipeline extracts a set of texture features from points on a spatial regular lattice, determined by two parameters: the window size and lattice distance. For each mammogram and each feature, our pipeline generates a feature image composed by feature values at all lattice points. (Examples of feature images are shown in Fig. 8.)

The analyzed features are organized into three groups, including (i) texture descriptors of gray-level histograms, (ii) co-occurrence features, and (iii) run length features. These texture features were used previously in breast cancer risk assessment studies[17, 19 20]. The current implementation of the texture feature extraction method includes two additional parameters defining the histogram bin number and pixel offset (for computing co-occurrence matrix). The selection of these parameters was guided by the previous studies[19]. In this study, 25 texture properties of phantom images were compared with those from clinical mammograms. We used a lattice distance of 31 pixels, a window size of 63 pixels, a co-occurrence offset of 5 pixels, and 100 bins for the estimation of texture feature histograms.

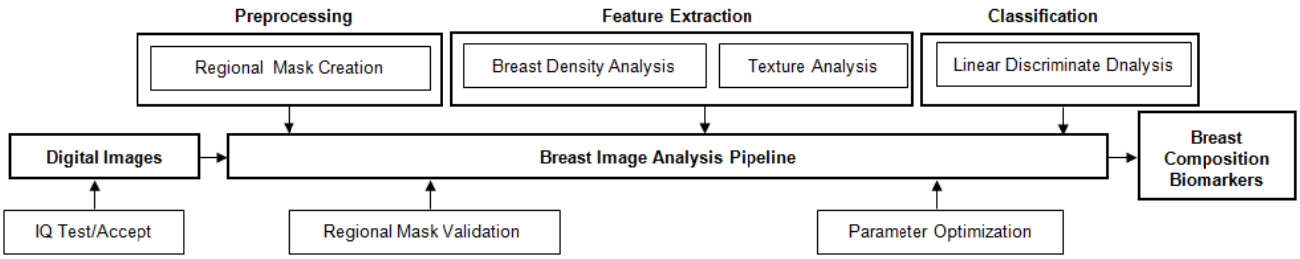

Figure 6: The flowchart of our fully-automated software pipeline for breast density and parenchymal texture analysis.

2.5. Statistical assessment of the agreement between clinical and phantom texture

For each of the 25 analyzed texture features, we estimated two types of histograms: (i) Mean histograms of feature values and (ii) Histograms of the mean feature values. Fig. 7 illustrates the difference between these 2 types of histograms.

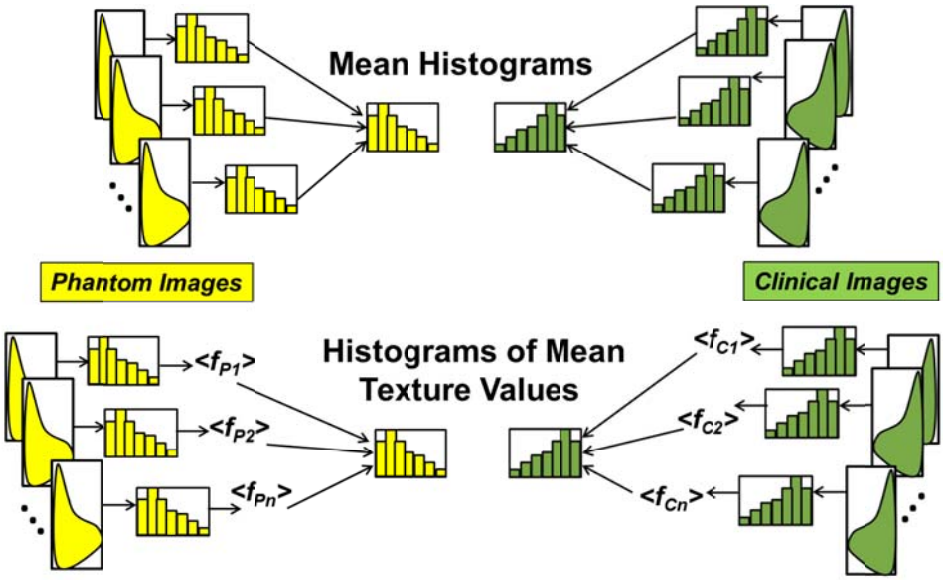

Figure 7: Two types of texture histograms compared in this paper between synthetic and clinical mammograms. Mean histograms (top) were calculated using pixel intensities of a texture image. In addition, we calculated histograms of the mean values from individual texture images (bottom).

The histogram comparison between clinical and synthetic texture properties was quantified using symmetrized Kulback-Leibler divergence:[13]

$$KL_{div}(P_1(x),P_2(x)) = \sum_x [P_1(x)\ log(P_1(x)/P_2(x))] \ .$$

Since KL_{div} is non-symmetric, we used a symmetrized version (also called Jensen-Shannon divergence[14]), which is locally proportional to the Fisher information metric:

$$KL_{div}^{\ sym} = [KL_{div}(P_1,Q) + KL_{div}(P_2,Q)]/2,$$

where $Q=(P_1+P_2)/2$. Separate assessments of the agreement with clinical data were made for images of software phantoms generated using octree and region growing simulation methods.

3. RESULTS AND DISCUSSION

3.1 Texture images

Fig. 8 shows examples of texture images calculated from synthetic (Fig. 8 (a) and (b)) and clinical (Fig. 8 (c) and (d)) mammograms. Shown are texture maps corresponding to features of Entropy (Fig.8 (a) and (c)) and Grey Level Non-Uniformity (Fig. 8 (b) and (d)).

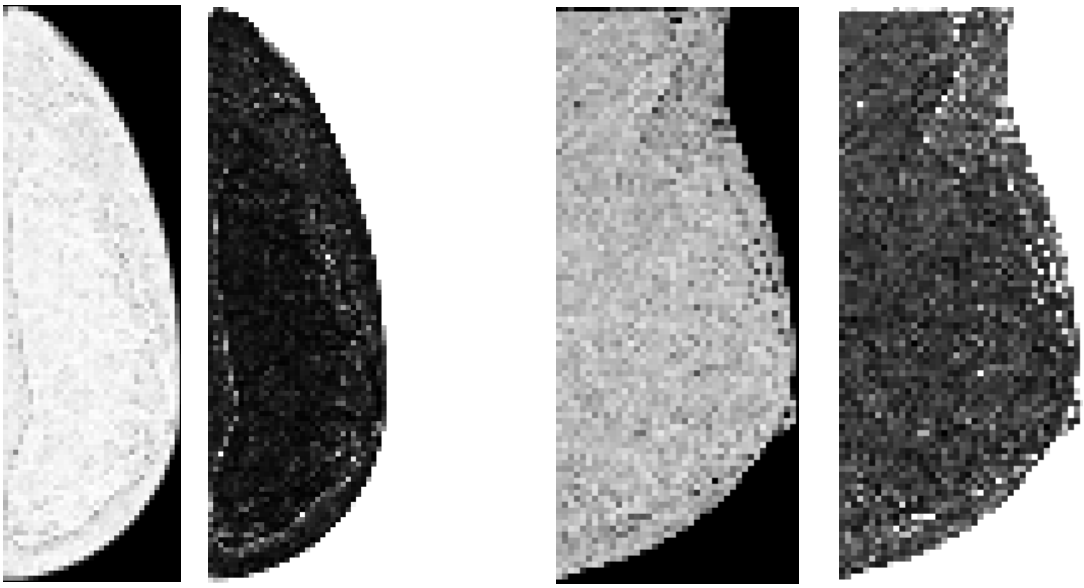

(a) (b) (a) (b)

Figure 8: An Entropy (a) and Grey Level Non-Uniformity (b) texture images, corresponding to the clinical mammogram (shown in Fig. 5). An Entropy (c) and Grey Level Non-Uniformity (d) texture images corresponding to the phantom mammogram (shown in Fig. 4).

3.2 Agreement between synthetic and clinical image texture properties

Fig. 9 shows examples of features in which there is good agreement between the mean histograms of clinical and synthetic mammogram texture properties. Shown are mean histograms of the High Grey Level Run Emphasis (Fig. 9 (a)) and the 5th Percentile (Fig. 9 (b)) features. Separate bars are shown for the texture features corresponding to the clinical data, octree phantoms and region growing phantoms. The good agreement is made evident by the high level of overlap between clinical and synthetic histograms, and is also supported by low KL_{div}^{sym} values (indicated in figures).

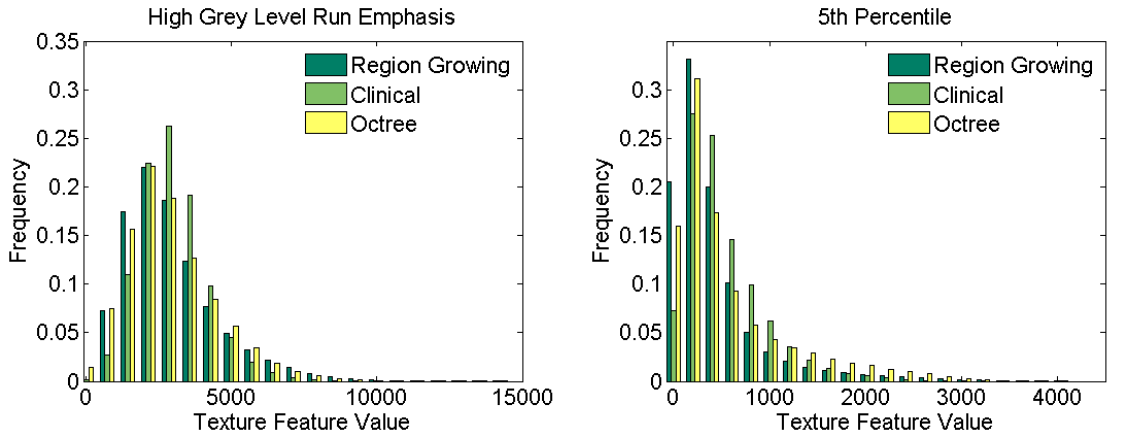

KL_{div}^{sym}: 0.031 (octree); 0.035 (reg. grow.) KL_{div}^{sym}: 0.041 (octree); 0.045 (reg. grow.)

Figure 9: Examples of a good agreement between mean histograms of clinical and synthetic texture features.

Fig. 10 illustrates good agreement between the histograms of mean values calculated from clinical and synthetic mammogram texture properties. Shown are the histograms of mean values of the High Grey Level Run Emphasis (Fig 10 (a)) and the 5th Percentile (Fig. 10 (b)) texture features. As compared to the mean histograms from Fig. 9, the histograms of mean texture values show higher KL_{div}^{sym} values.

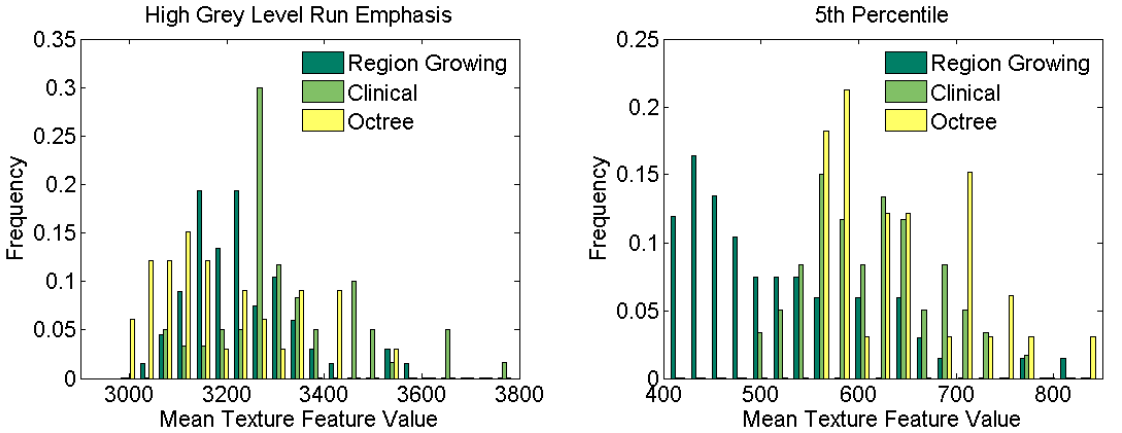

KL_{div}^{sym}: 0.419 (octree); 0.290 (reg. grow.) KL_{div}^{sym}: 0.173 (octree); 0.487 (reg. grow.)

Figure 10: Examples of a good agreement between histograms of mean clinical and synthetic texture features.

Figs. 11 and 12 show examples of texture features for which the octree phantoms yielded better agreement with clinical data as compared to the region growing method. Shown are mean histograms (Fig. 11) and the histograms of mean values (Fig. 12) of the Correlation and Cluster Shade texture features. As seen in Fig. 11, the octree mean histogram values are slightly closer to the clinical data, as compared to the region growing histograms. The histograms of mean texture features showed very similar performance of the octree and region growing phantoms.

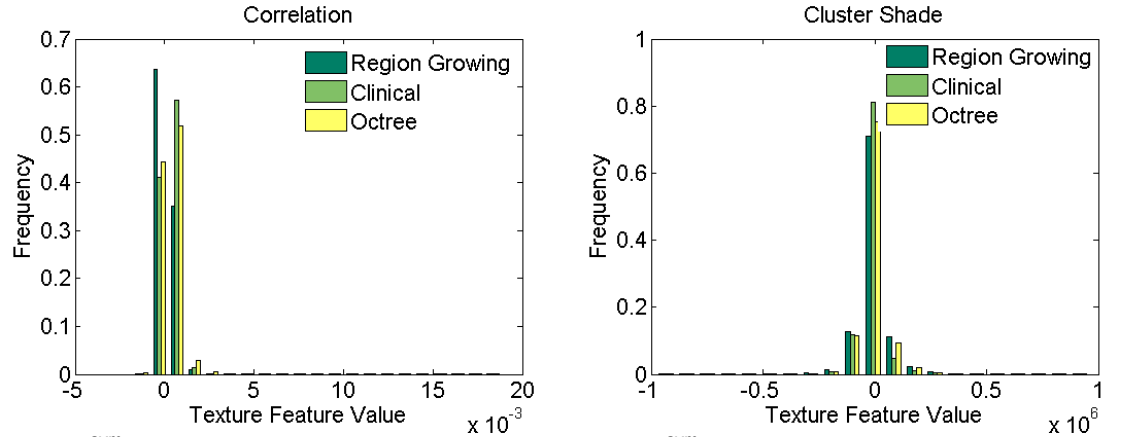

KL_{div}^{sym}: 0.006 (octree); 0.037 (reg. grow.) KL_{div}^{sym}: 0.008 (octree); 0.016 (reg. grow.)

Figure 11: Examples of the mean texture histograms for which octree phantoms yielded better agreement with clinical data than region growing phantoms.

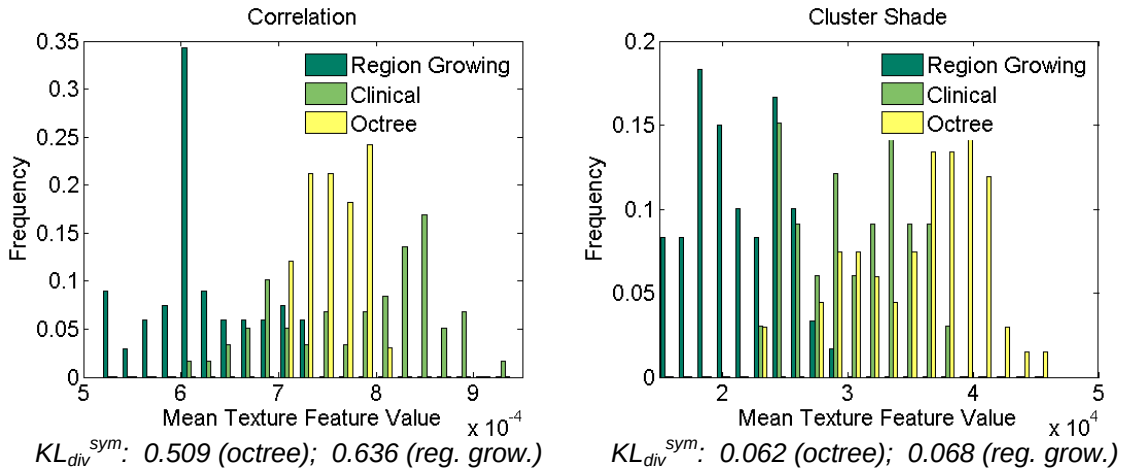

KL_{div}^{sym}: 0.509 (octree); 0.636 (reg. grow.) KL_{div}^{sym}: 0.062 (octree); 0.068 (reg. grow.)

Figure 12: Examples of the histograms of mean texture features for which octree phantoms yielded better agreement with clinical data than region growing phantoms.

We have also observed several texture features for which the region growing phantoms yielded better agreement with clinical data than octree-based simulation, as illustrated in Figs. 13 and 14. Shown are mean histograms (Fig. 13) and the histograms of mean values (Fig. 14) of the Low Gray Level Run Emphasis and Short Run Emphasis texture features. The advantage of the region growing phantoms may be caused, again, by mean histogram values being slightly closer to the clinical data, as compared to the octree phantoms (Fig. 13 left). In addition, we observed that for certain features there is practically no overlap between the histograms of octree–based and clinical texture properties (Fig. 13 right).

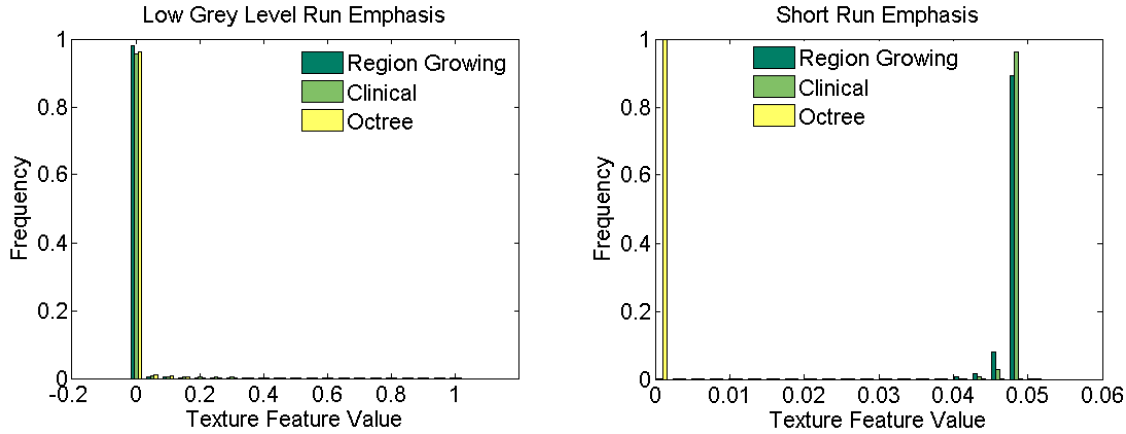

KL_{div}^{sym}: 0.006 (octree); 0.003 (reg. grow.) KL_{div}^{sym}: 1.000 (octree); 0.014 (reg. grow.)

Figure 13: Examples of the mean texture histograms for which region growing phantoms yielded better agreement with clinical data than octree phantoms.

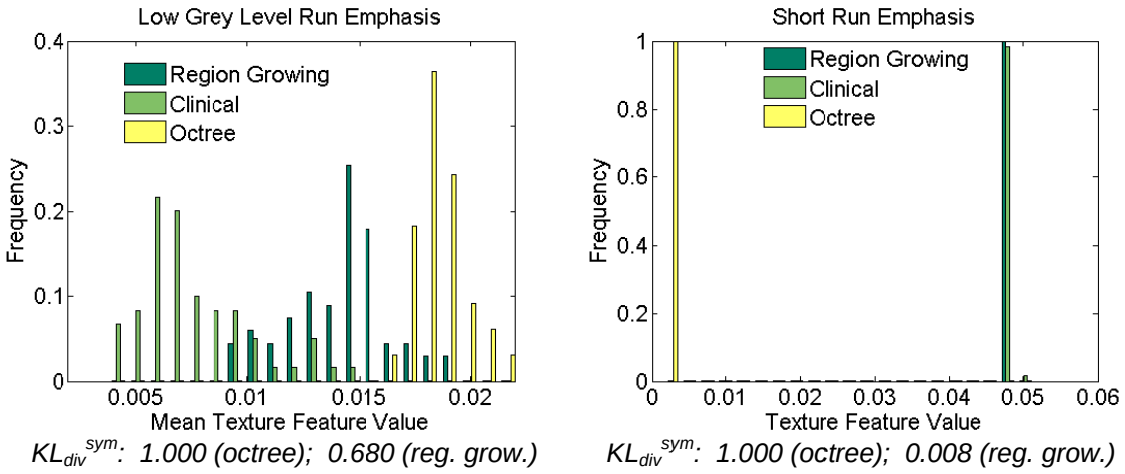

Figure 14: Examples of the histograms of mean texture features for which region growing phantoms yielded better agreement with clinical data than octree phantoms.

Fig. 15 and Table 1 show a review of all the 25 analyzed texture descriptors. Better agreement is indicated by lower KL_{div}^{sym} values. It can be seen that the octree and region growing phantoms yielded comparable agreement with clinical data. Octree phantoms showed better agreement (*highlighted in Table 1*) for 14 of 25 mean feature histograms, and for 15 of 25 histograms of mean texture features. In addition, octree-based approach offers a much faster simulation of phantoms with small voxel size.

As previously noticed the mean histograms show about an order of magnitude lower KL_{div}^{sym} values, as compared to the histograms of mean feature values. This suggests that a higher level of agreement with clinical data was observed for the simulated features averaged over the whole images and a larger number of women, as opposed to the features calculated from individual women and compared to individual clinical data. This observation is not surprising as for the purpose of this study we have not attempted to match the anatomical properties of software phantoms with the selected clinical data. Our goal in the future phantom studies is to use the similarity in texture features for guiding the software phantom design to improve matching with desired clinical populations.

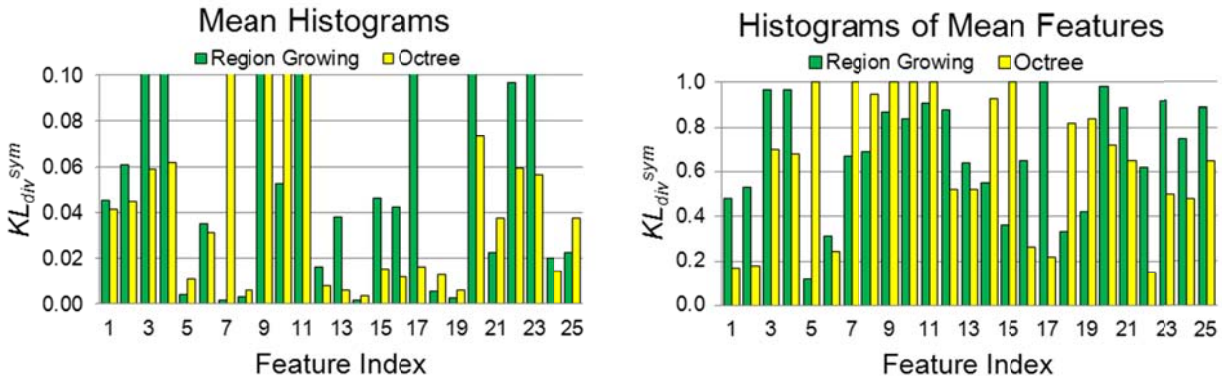

Figure 15: KL_{div}^{sym} values between synthetic and clinical mean texture histograms (left) and histograms of mean texture features (right) for all 25 analyzed texture features. Separately shown are KL_{div}^{sym} values for octree phantoms (light yellow) and region growing phantoms (dark green).

Table 1: Percent differences in square root KL_{div}^{sym} values of octree vs. region growing phantom images for all 25 analyzed features. Highlighted are features for which octree phantoms showed better agreement with clinical data than region growing phantoms.

Index	Texture Feature	Mean Histogram	Histogram of Mean
		$\Delta(KL_{div}^{sym})^{0.5}$ [%]	$\Delta(KL_{div}^{sym})^{0.5}$ [%]
1	5th Percentile	-4.30	-35.14
2	5th Mean	-14.33	-42.50
3	95th Percentile	-25.96	-13.57
4	95th Mean	-30.63	-13.75
5	Gr.Lev. Nonuniformity	73.21	265.64
6	High Gr.Lev. Run Emphasis	-5.74	20.17
7	Long Run Emphasis	3426.68	*
8	Low Gr.Lev. Run Emphasis	41.42	21.28
9	Run Length Nonuniformity	126.49	16.37
10	Run Percentile	467.92	35.18
11	Short Run Emphasis	757.49	991.09
12	Cluster Shade	-30.40	-73.56
13	Correlation	-60.57	-10.55
14	Energy	47.53	23.74
15	Entropy	-41.82	89.95
16	Haralick Correlation	-47.25	-41.12
17	Offset 5 Inertia	-62.47	-61.10
18	Inverse Difference Moment	-52.21	90.87
19	Kurtosis	56.79	53.62
20	Max	-32.67	-12.64
21	Mean	28.81	-12.95
22	Min	-21.58	-59.87
23	Sigma	-52.74	-22.79
24	Skewness	-23.38	-8.64
25	Sum	28.81	-12.95

4. CONCLUSIONS

We have evaluated an automated analysis of texture properties in synthetic mammograms generated using software breast phantoms. This work is motivated by the development of an automated tool for realism testing in an open source platform for breast imaging simulations. Texture properties of mammograms synthesized using our software phantoms showed relatively good agreement with clinical data. Better agreement was observed for mean histograms of texture features vs. histograms of mean texture features. Phantoms generated by the octree and region growing methods have comparable agreement with clinical data. The octree based method offers an additional advantage of very fast generation of phantoms with small voxel size.

Our future studies will focus on improving our understanding of the texture features that showed lower agreement between synthetic and clinical images, in order to inform further modifications of the software phantom design to improve realism. In addition, the effect of simulating small scale tissue variations (e.g., using approaches developed by Reiser *et al.* [21-23] or Bliznakova *et al.* [7]) on texture properties will be analyzed. We are also interested in extending the performed texture analysis to include synthetic breast tomosynthesis images.

ACKNOWLEDGMENT

This work was supported in part by the US National Institutes of Health (R21 grant #CA155906-01A1 and R01 grant #CA154444) and the US National Science Foundation (IIS-0916690). We are grateful to Barry Ren and Andy Smith of HOLOGIC for providing processed phantom images and to Joseph Chui, Roshan Karunamuni, and David Pokrajac for their help with phantom image simulation and data analysis.

REFERENCES

1. Bakic PR, Albert M, Brzakovic D, Maidment ADA. Mammogram synthesis using a 3D simulation. I. Breast tissue model and image acquisition simulation. *Medical Physics.* 2002;29(9):2131-2139.

2. Bakic PR, Albert M, Brzakovic D, Maidment ADA. Mammogram synthesis using a 3D simulation. II. Evaluation of synthetic mammogram texture. *Medical Physics.* 2002;29(9):2140-2151.

3. Bakic PR, Albert M, Brzakovic D, Maidment ADA. Mammogram synthesis using a three-dimensional simulation. III. Modeling and evaluation of the breast ductal network. *Medical Physics.* 2003;30(7):1914-1925.

4. Bakic PR, Brzakovic D. Simulation of digital mammogram acquisition. Paper presented at: SPIE Medical Imaging: Physics of Medical Imaging, 1999; San Diego, CA.

5. Bakic PR, Brzakovic D, Brzakovic P, Zhu Z. An Approach to Using a Generalized Breast Model to Segment Digital Mammograms. *11th Symposium on Computer-Based Medical Systems*. Lubbock, TX; 1998:84-89.

6. Bakic PR, Brzakovic D, Zhu Z. Anatomic Segmentation of Mammograms via Breast Model. In: Kerssemeijer ea, ed. *4th International Workshop on Digital Mammography*. Nijmegen, The Netherlands: Kluwer, Dordrecht; 1998:291-294.

7. Bliznakova K, Suryanarayanan S, Karellas A, Paiilikarakis N. Evaluation of an improved algorithm for producing realistic 3D breast software phantoms: Application for mammography. *Medical Physics.* 2010;37(11):5604-5617.

8. Hoeschen C, Fill U, Zankl M, Panzer W, Regulla D, Dohring W. A high resolution voxel phantom of the breast for dose calculations in mammography. *Radiation Protection Dosimetry* 2005;114(1-3):406-409.

9. Li CM, Segars WP, Lo JY, Veress AI, Boone JM, Dobbins III JT. Computerized 3D Breast Phantom with Enhanced High-Resolution Detail. In: Samei E, Hsieh J, eds. *SPIE Medical Imaging: Physics of Medical Imaging* Vol 7258. Lake Buena Vista, FL 2009.

10. Chen B, Shorey J, Saunders RSJ, et al. An anthropomorphic breast model for breast imaging simulation and optimization. *Academic Radiology.* 2011;18(5):536-546.

11. O'Connor JM, Das M, Didier C, Mah'D M, Glick SJ. Development of an Ensemble of Digital Breast Object Models. In: Marti J, ed. *Digital Mammography (IWDM).* Vol 6136. Berlin-Heidelberg: Springer-Verlag; 2010:54-61.

12. Pokrajac DD, Maidment ADA, Bakic PR. Optimized generation of high resolution breast anthropomorphic software phantoms. *Medical Physics.* 2012;39(4):2290-2302.

13. Kullback S. Letter to the Editor: The Kullback–Leibler distance. *The American Statistician* 1987;41(4):340-1.

14. Lin J. Divergence measures based on the shannon entropy. *IEEE Transactions on Information Theory.* 1991;37(1):145-151.

15. Zhang C, Bakic PR, Maidment ADA. Development of an Anthropomorphic Breast Software Phantom Based on Region Growing Algorithm. Paper presented at: SPIE Medical Imaging, 2008; San Diego, CA.

16. Bakic PR, Zhang C, Maidment ADA. Development and Characterization of an Anthropomorphic Breast Software Phantom Based upon Region-Growing Algorithm. *Medical Physics.* 2011;38(6):3165-3176.

17. Zheng Y, Keller B, Wang Y, et al. A Fully-Automated Software Pipeline for Parenchymal Pattern Analysis in Digital Breast Images: Towards the Translation of Imaging Biomarkers in Routine Breast Cancer Risk Assessment. Paper presented at: RSNA, 2011; Chicago, IL.

18. Zheng Y, Wang Y, Keller BM, Conant EF, Gee JC, Kontos D. A fully-automated software pipeline for integrating breast density and parenchymal texture analysis for digital mammograms: Parameter optimization in a case-control breast cancer risk assessment study. In: Nishikawa RM, Whiting BR, eds. *SPIE Medical Imaging*. Lake Buena Vista, FL: SPIE; 2013.

19. Wang Y, Keller BM, Zheng Y, et al. A Phantom Study for Assessing the Effect of Different Digital Detectors on Mammographic Texture Features. Digital Mammography. In: Maidment ADA, Bakic PR, Gavenonis SC, eds. *International Workshop on Breast Imaging (IWDM)*. Philadelphia, PA: Springer; 2012.

20. Wang Y, Keller BM, Zheng Y, et al. Texture feature standardization in digital mammography for improving generalizability across devices. *SPIE Medical Imaging*. San Diego, CA; 2012.

21. Reiser I, Nishikawa RM. Task-based assessment of breast tomosynthesis: Effect of acquisition parameters and quantum noise *Medical Physics.* 2010;37(4):1591-1600.

22. Lau AB, Reiser I, Nishikawa RM, Bakic PR. A statistically defined anthropomorphic software breast phantom *Medical Physics.* 2012;39(6):3375-3385.

23. Reiser I, Lau AB, Nishikawa RM, Bakic PR. A directional small-scale tissue model for an anthropomorphic breast phantom. *International Workshop on Breast Imaging*. Philadelphia, PA: Springer; 2012.